Statistical Fluctuations in Heavy-Ion Collisions

L. G. MORETTO

Nuclear Science Division, Lawrence Berkeley Laboratory
University of California, Berkeley, CA 94720

Abstract: The relevance of the statistical equilibrium limit to the description of substantially relaxed degrees of freedom is discussed. Fluctuations are considered specifically in the following processes: the correlation between entrance-channel angular momentum and exit-channel kinetic energy; the sharing of the dissipated kinetic energy between the two fragments; the magnitude and the alignment of the fragment angular momentum including the effect of shell structure. It is found that statistical fluctuations play a major role and that the statistical equilibrium limit seems to have been reached for a number of degrees of freedom.

LBL--14137

DE82 012911

This work was supported by the Director, Office of Energy Research, Division of Nuclear Physics of the Office of High Energy and Nuclear Physics and by Nuclear Sciences of the Basic Energy Sciences Program of the U.S. Department of Energy under Contract DE-AC03-76SF00098.

1. Introduction

Fluctuations may originate either in quantal or in statistical effects, and may be associated either with equilibrium or nonequilibrium processes. Their relevance becomes preeminent when the temperature T (or the phonon $\hbar\omega$) becomes comparable with the potential energy variations ΔV along a given collective coordinate. When this occurs, the second and higher moments of the resulting distributions become important. Furthermore, spectral distributions are frequently controlled, more or less directly, by fluctuations (e.g., kinetic energy spectra). Finally, the dissipation-fluctuation theorem states that fluctuations are the inevitable consequence of dissipative processes (frictional terms), thus setting a physical limit to the validity of trajectory calculations.

The question of quantal versus thermal fluctuations is an interesting one. The former has been pursued theoretically by the Copenhagen group[1]; the latter has such a solid historical tradition in the field of the compound nucleus decay that it is not in need of strong justification. The question of nonequilibrium vs. equilibrium fluctuations is worth debating in some greater detail.

We shall limit our discussion to equilibrium statistical fluctuations, for the following reason. Let us assume that the approach to equilibrium is controlled by a diffusive process as described by the Master Equation or by the Langevin equation. Furthermore, let us assume that the system is harmonically bound along the coordinate under consideration, namely:

$$V(x) = \frac{1}{2}cx^2$$

If we start from $x = x_0$ at $t = 0$ with a delta function distribution, after a time t the distribution is a Gaussian with centroid and width given by:

$$\begin{aligned} x &= x_0 e^{-cBt} \\ \sigma^2 &= \frac{T}{c}\left(1 - e^{-2cBt}\right) \end{aligned} \qquad (1)$$

where B is the "mobility" of the system. After one relaxation time $\tau = 1/cB$, we have:

$$\frac{x}{x_0} = e^{-1} = 0.368 \quad ; \frac{\sigma}{\sigma_{equil}} = 1 - \frac{1}{2}e^{-2} = 0.93$$

This means that, while, after one relaxation time, the centroid is still 37% of the initial distance from equilibrium, the width is already 93% of the final equilibrium value. In other words, the width grows rapidly towards its equilibrium value independently of the starting point and can approach its limiting value while the

mean may still be quite far away from equilibrium. Even after only one-half the relaxation time, the width is already 82% of its equilibrium value, while the mean is still 60% of the initial distance from equilibrium. Consequently, if the system has any inclination at all to relax towards equilibrium, we can estimate the fluctuations quite reliably by means of the equilibrium fluctuations without worrying too much about the time dependence of the process. Of course, the time dependence is a very important feature that deserves to be studied in detail. However, if we are concerned about the role of fluctuations and about their ability to scramble the experimental picture, a thorough investigation of the equilibrium limit is the most economical way to obtain information about this problem.

In what follows, I would like to give some examples of the role of fluctuations in deep inelastic processes. In particular, I shall discuss: a) fluctuations in the exit channel kinetic energy and the correlation (or the lack of it) between it and the entrance channel angular momentum, b) fluctuations in the partition of the dissipated energy between the two fragments and their possible effects in the emission of fast particles, c) the effect of shell structure on the first and second moment of the fragment spins and d) fluctuations in the spin components of the fragments and the resulting spin misalignment as observed from sequential fission and γ-ray decay of the fragments.

2. Fluctuations in exit-channel kinetic energy at fixed entrance-channel angular momentum

It would be highly desirable and useful to find a way of inferring the entrance-channel angular momentum from some easily measurable exit-channel observable, like the kinetic energy. While some correlation between these quantities is obviously present, especially in the quasi-elastic region, fluctuations of a various nature tend to spoil it to a serious degree. We are going to discuss two sources of fluctuations relevant to this problem: a) the coupling of the orbital motion to a thermally excited wriggling mode;[3]) and b) the effect of random shape fluctuations at scission.

2a) COUPLING OF THE ORBITAL MOTION TO ONE WRIGGLING MODE

Let us consider the simple analytical case of two equal touching spheres with one wriggling mode[3]) coupled to the orbital motion.

The exit channel kinetic energy above the Coulomb barrier is:

$$E = \frac{l^2}{2\mu d^2} \qquad (2)$$

where l is the exit-channel orbital angular momentum, μ is the reduced mass, and d is the distance between centers, equal to the sum of the radii.

The total rotational energy is:

$$E_R = \frac{l^2}{2\mathcal{J}^*} + \frac{I^2}{4\mathcal{J}} - \frac{Il}{2\mathcal{J}} \qquad (3)$$

where I is the entrance channel angular momentum, $\mathcal{J}$ is the moment of inertia of one of the two spheres, and $\mathcal{J}^{*-1} = (\mu d^2)^{-1} + (2\mathcal{J})^{-1}$ or $\mathcal{J}^* = 10/7\,\mathcal{J}$. In the limit of thermal equilibrium, the l distribution is:

$$P(l)dl = (2\pi\mathcal{J}^*T)^{-1/2} \exp -\left(\frac{l^2}{2\mathcal{J}^*T} - \frac{Il}{2\mathcal{J}T} + \frac{I^2\mathcal{J}^*}{8\mathcal{J}^2T}\right) \qquad (4)$$

where T is the temperature. Introducing a $2ldl$ weight and the dimensionless variables $\varepsilon = E/T$, $\lambda = l/(\mathcal{J}T)^{1/2}$, we obtain the distribution function

$$P(\varepsilon,\lambda)d\varepsilon d\lambda = \frac{\lambda}{\sqrt{\varepsilon}} \exp -\left[\frac{7}{2}\varepsilon - \sqrt{\frac{5}{2}}\,\lambda\,\sqrt{\varepsilon} + \frac{5}{28}\lambda^2\right] d\varepsilon d\lambda \quad . \qquad (5)$$

The properties of this distribution function can be observed in the two-dimensional plot in fig. 1 and can be summarized as follows.

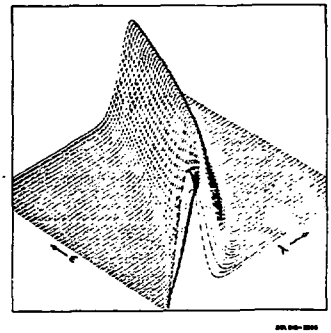

Fig. 1. Two-dimensional plot of the distribution function given in eq. 5.

At constant ϵ (a fixed cut in the exit channel kinetic energy), the most probable value of λ is:

$$\hat{\lambda} = \frac{7}{\sqrt{10}} \sqrt{\epsilon}\left[1 + \sqrt{1 + \frac{4}{7\epsilon}}\right] \tag{6}$$

to be compared with

$$\lambda = \frac{14}{\sqrt{10}} \sqrt{\epsilon} \text{ from simple dynamics,}$$

while the width is given by

$$\sigma^2 = \frac{14}{5} \text{ , independent of } \epsilon! \tag{7}$$

Since $\mathcal{J}T$ is typically 100–200 $\hbar^2$, we have widths in the entrance channel angular momentum

$$17\hbar \leq \sigma \leq 24\hbar$$

$$40\hbar \leq \Gamma_{FWHM} \leq 56\hbar$$

for an infinitely sharp cut in the exit channel kinetic energy.

At constant λ (a fixed entrance-channel angular momentum), the average kinetic energy over the barrier is:

$$\bar{\epsilon} = \frac{2}{7}\left(\frac{1}{2} + \frac{5}{28}\ \lambda^2\right) \tag{8}$$

while the width is:

$$\sigma^2 = \frac{4}{49}\left(\frac{1}{2} + \frac{5}{14}\lambda^2\right) \qquad (9)$$

and

$$\frac{\sigma}{\varepsilon} = \frac{(1/2 + 5/14\lambda^2)^{1/2}}{1/2 + 5/28\ \lambda^2} \underset{\text{large } \lambda}{\simeq} 2\sqrt{\frac{14}{5}}\frac{1}{\lambda} \quad . \qquad (10)$$

For an entrance channel angular momentum I = 240ħ , $\mathcal{J}_T = 144\hbar^2$, T = 3 MeV, one obtains

σ = 10 MeV

Γ_{FWHM} = 23.5 MeV,

while, for I = 360ħ (lrms for Ho + Ho at 8.5 MeV/A) one obtains:

σ = 15 MeV

Γ_{FWHM} = 36 MeV.

Examples of distributions in ε at fixed λ are shown in fig. 2. The conclusion is that a sizeable mixing of entrance channel l-waves is predicted for a fixed exit-channel kinetic energy by invoking just one thermally-excited wriggling mode.

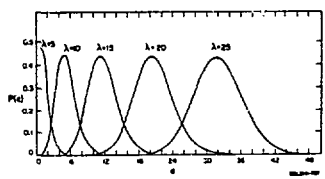

Fig. 2. Kinetic energy distributions for various values of the entrance-channel angular momentum.

We conclude this subject by calculating the kinetic energy distribution integrated over angular momentum from 0 to λ_{mx}. The integration yields:

$$P(\varepsilon) \propto \frac{1}{\sqrt{\varepsilon}}\left[e^{-\frac{7}{2}\varepsilon}\left\{1 - e^{-\frac{5}{28}\lambda_{mx}^2 + \sqrt{\frac{5}{2}}\lambda_{mx}\sqrt{\varepsilon}}\right\} + \sqrt{\frac{7\pi}{2}}\sqrt{\varepsilon}\left\{\operatorname{erf}\left(\sqrt{\frac{5}{28}}\lambda_{mx} - \sqrt{\frac{7}{2}}\sqrt{\varepsilon}\right) + \operatorname{erf}\sqrt{\frac{7}{2}}\sqrt{\varepsilon}\right\}\right] \quad . \qquad (11)$$

Plots of this distribution for different values of λ_{mx} are shown in fig. 3. In order to appreciate better this result, we can calculate the corresponding distribution in the absence of fluctuations (T = 0) in the limit of rigid rotation:

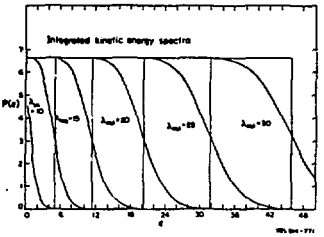

Fig. 3. Angular-momentum-integrated kinetic energy distributions for different values of the maximum angular momentum. The box-like distributions defined by the vertical lines are obtained by eliminating fluctuations.

The kinetic energy over the barrier is:

$$E = \frac{l^2}{2\mu d^2} = \frac{25}{49}\frac{I^2}{2\mu d^2}$$

which implies

$$dE \propto dI^2.$$

But, from the entrance channel distribution, we have

$$P(l)dl = K2ldl = Kdl^2 = k'dI^2,$$

then

$$P(E)dE \propto dI^2 \propto dE \qquad 0 \leq I \leq I_{mx}$$

or, more precisely,

$$P(\varepsilon)d\varepsilon = \begin{cases} Kd\varepsilon & \varepsilon \leq \frac{5}{98}\lambda_{mx}^2 \\ 0 & \varepsilon > \frac{5}{98}\lambda_{mx}^2 \end{cases}.$$

In other words, we have a rectangular distribution. Examples of such distributions are also shown in fig. 3.

2b) EFFECT OF SHAPE FLUCTUATIONS ON THE EXIT CHANNEL KINETIC ENERGY

It it well known that the observed sub-Coulomb emission of deep-inelastic fragments is due to their sizeable deformation at the scission point. The reasonably flat dependence of the total potential energy at scission as a function of deformation, together with the rather steep dependence of the two-fragment Coulomb interaction, leads to the possibility of fairly large shape fluctuations at scission with a resulting amplification of the fluctuations in the kinetic energy at infinity.[4])

For sake of simplicity, let us model the system at scission as composed of two equal and equally deformed spheroids in contact. The relevant total potential energy is

$$V_T = V_S(\epsilon) + V_C(\epsilon) + V_{Rot}(I,\epsilon) \qquad (12)$$

where V_S, V_C, V_{Rot} are the surface, Coulomb, and rotational energy, respectively; ϵ is the common deformation of the spheroids; and I is the angular momentum. In our model the potential energy has a minimum at a deformation ϵ_0 defined by

$$\frac{\partial V_T}{\partial \epsilon} = 0.$$

The potential energy can be expanded quadratically about the minimum as

$$V_T = V_0 + k(\epsilon - \epsilon_0)^2 \quad . \qquad (13)$$

Similarly, the resulting kinetic energy at infinity is given by

$$E_{kin} = V_C^*(\epsilon) + \frac{I(\epsilon)^2}{2\mu d^2(\epsilon)} \qquad (14)$$

where V_C^* is the two-fragment Coulomb interaction, $l(\epsilon)$ is the orbital angular momentum at scission determined from the rigid rotation condition, and d is the center-to-center distance. A linear expansion in ϵ about ϵ_0 leads to

$$E_{Kin} \simeq E^R_{in}(\epsilon_0) + c(\epsilon - \epsilon_0) \quad .$$

From fig. 4, one sees that a small (energy-wise) fluctuation at scission, of the order of 1/2T in the thermal limit, leads to an amplified fluctuation in the final kinetic energy, so that

$$\sigma^2_{Kin} = \frac{c^2}{2k}T = \frac{pT}{2} \qquad (15)$$

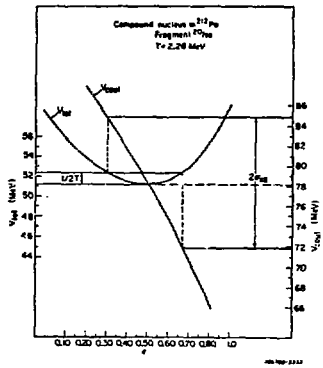

Fig. 4. Amplification of fluctuations at scission illustrated for a ^{20}Ne emitted by the compound system ^{212}Po.

where p is called the amplification parameter.[4]) The exit-channel kinetic energy distribution is, in fact, approximately a Gaussian

$$P(E_{Kin}) \propto \exp - \frac{(E_{Kin}-E^{o}_{Kin})^2}{p\bar{T}} \quad . \qquad (16)$$

Certainly a great deal of the width in the final kinetic energy distribution arises from this effect. Even more interesting is the fact that the large spread in final kinetic energy is associated with a fixed total angular momentum. Of course, this feature has the effect of spreading any given l-wave over a very broad range of kinetic energies, thus making the correlation between exit-channel kinetic energy and entrance-channel angular momentum very problematic.

As an example, let us consider the system Fe + Fe. In fig. 5 the kinetic energy distributions are shown for a set of l values. While the centroid of the distribution moves towards higher values with increasing l, the width also increases, leading to a dramatic overlap of distributions with widely different l-values. Most interesting are the entrance-channel angular momentum distributions for a variety of exit-channel kinetic energies shown in fig. 6. The distributions are so broad that at any kinetic energy the whole l-wave spectrum is substantially sampled. The overall features of the distribution are shown by the two-dimensional plot in fig. 7.

In conclusion, we have seen how the two processes described in a) and b) have the effect of spoiling the correlation between entrance-channel angular momentum and exit-channel kinetic energy.

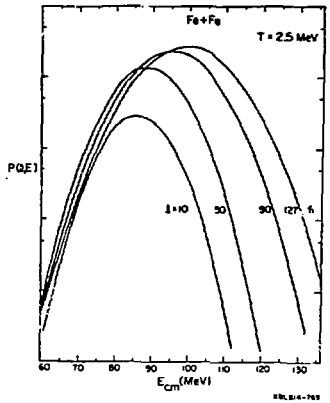

Fig. 5. Kinetic energy spectra for various values of the entrance-channel angular momentum for the system Fe + Fe.

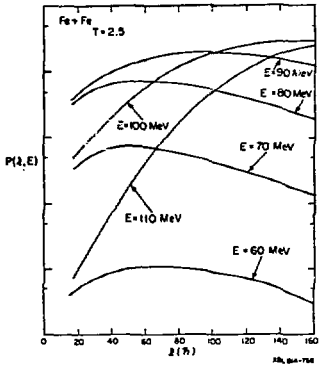

Fig. 6. Entrance-channel angular momentum distributions for various values of exit-channel kinetic energies.

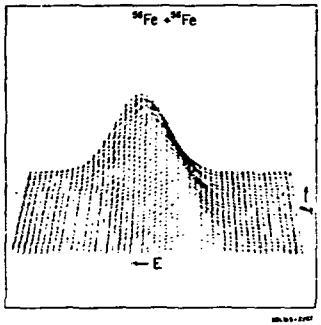

Fig. 7. Two-dimensional plot of the emission probability as a function of entrance-channel angular momentum and exit-channel kinetic energy.

3. Energy partition between the two fragments

The partition of excitation energy between the partners in a deep-inelastic collision (DIC) appears to reach equilibrium on a very short time scale. This is shown by the experimental observation that the mean number of evaporated particles from coincident reaction products is proportional to the fragment masses,[5-7]) as required by the thermal equilibrium condition. Moreover, this proportionality is found for the entire range of dissipated energy, up to the smallest energy losses[8-10]) (i.e., the shortest collision times). Thus the thermalization time must be shorter than the shortest interaction times. A further check of complete statistical equilibrium can be made by observing statistical fluctuations in the division of the excitation energy between the two fragments.[11]) Such fluctuations will have important consequences for the reaction products. The effects of a fluctuating excitation energy division on evaporation spectra and the disguising of pre-equilibrium components have been described recently by Schmitt et al.[12]).

In this section we evaluate the magnitude of statistical fluctuations in the energy partition in DIC and explore two avenues through which the calculated fluctuations can manifest themselves, namely neutron energy spectra and evaporated neutron number.[13]) We find that these two observables are complementary in that statistical fluctuations have a large effect on the neutron energy spectra when the mass asymmetry is large but have a relatively small effect for equal fragments. Fluctuations also introduce a covariance in the number of evaporated nucleons which is most prominent for equal fragments.

The statistical weight associated with a given partition of the total excitation energy, E, between two fragments in statistical equilibrium is proportional to the product of their level densities:

$$P(x)\,dx \propto \rho_1(x)\,\rho_2(E-x)\,dx \quad . \tag{17}$$

The equilibrium condition is given by:

$$\frac{d}{dx}\ln P(x) = 0 = \frac{d}{dx}\ln \rho_1(x) + \frac{d}{dx}\ln \rho_2(E-x) = \frac{1}{T_1} - \frac{1}{T_2} \tag{18}$$

The terms on the right-hand side of eq. 18 are the reciprocals of the fragment's temperatures and their equality immediately requires the excitation energy to divide in proportion to the mass ratio:

$$\frac{E_1^*}{E_2^*} = \frac{x}{E-x} = \frac{A_1}{A_2} \quad . \tag{19}$$

The expansion of the logarithm of the probability distribution about the maximum up to 2nd order gives a Gaussian:

$$P(x)\,dx \propto e^{-(x_o-x)^2/2\sigma^2} \qquad (20)$$

thus

$$\frac{1}{\sigma^2} = -\frac{d^2}{dx^2}\ln P(x) = \frac{d}{dx}\left(\frac{1}{T_1}\right)_T + \frac{d}{dx}\left(\frac{1}{T_2}\right)_T$$
$$= \frac{1}{T^2}\left(\frac{1}{C_{V1}} + \frac{1}{C_{V2}}\right) \qquad (21)$$

where C_{V1} and C_{V2} are the heat capacities of the two fragments (for a Fermi gas $C_V = 2aT$ at a temperature T). On substitution we obtain for the width:

$$\sigma^2 = 2T^3\,\frac{a_1 a_2}{a_1 + a_2} \qquad (22)$$

where a_1 and a_2 are the level density parameters of the fragments.

A direct way in which any fluctuations in the excitation energy of DIC fragments can be observed is in the energy spectra of evaporated nucleons.

For a very asymmetric system, the magnitude of the fluctuations is comparable to the total excitation energy of the light fragment and therefore produces an important change in the spectrum.

As an applied example, fig. 8 shows the proton spectra in coincidence with deep inelastic fragments for the reaction Ne + Cu at 252 MeV.[12]) While the hard spectrum could be attributed to prompt emission, it is in fact explained quite simply by energy fluctuations (solid lines) while it is not consistent with fixed energy splitting between fragments (dashed lines).

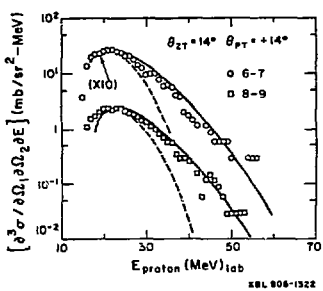

Fig. 8. Proton spectra in coincidence with deep inelastic processes for the reaction 252 MeV ^{20}Ne + ^{nat}Cu. The dashed lines are evaporation calculations without fluctuations in the energy partition. The solid lines incorporate the fluctuations.

A less direct, but more dramatic effect of excitation energy fluctuations can be seen in the number of nucleons evaporated from the pair of DIC fragments. An anticorrelation in the excitation energies of reaction partners naturally arises when the total excitation energy is held constant. The covariance of the number of emitted neutrons from DIC partners was investigated with a simple Monte Carlo code. The division of the excitation energy between symmetric fragments ($A = 100$) was either fixed or picked at random in proportion to eq. 17. The two fragments were then allowed to emit neutrons until the nuclei had cooled to less than $B_N + 2T'$, where B_N is the liquid drop neutron binding energy and T' is the temperature after emission of the previous neutron. The probability contours for emission of ν_1 neutrons from fragment 1 and ν_2 neutrons from fragment 2 are shown in fig. 9. When the fluctuations are turned on, a strong correlation between ν_1 and ν_2 is introduced.

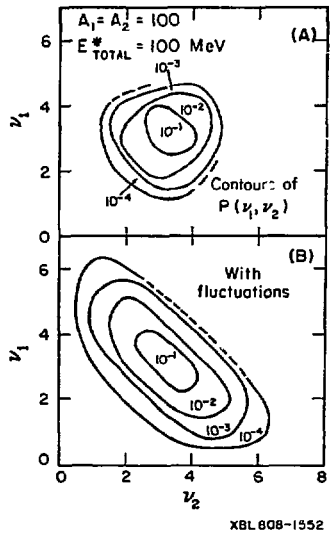

Fig. 9. Probability distribution for the number of neutrons emitted by the two fragments for a Q-value of -100 MeV. The fluctuations in the energy partition are incorporated in B.

4. Angular momentum fluctuations

Let us consider a frame of reference where the z axis is parallel to the entrance-channel angular momentum, the x axis is parallel to the recoil direction of one of the fragments, and the y axis is perpendicular to the z,x plane.

If the intermediate complex is assumed to have the shape of two equal touching spheres, the angular-momentum-bearing normal modes are easily identifiable. We shall call them "bending," B (doubly degenerate), "twisting" Tw (degenerate with bending), "wriggling" W (doubly degenerate) and "tilting" Ti.

In a recent work, the statistical mechanical aspects of the excitation of these modes have been studied in detail.[3]

The thermal excitation of these collective modes leads to Gaussian distributions in the three angular momentum components I_x, I_y, I_z.

4a) GAMMA RAY MULTIPLICITIES AND ANGULAR DISTRIBUTIONS

The fragment angular momentum is removed mainly by stretched E2 decay. The alignment of the angular momentum should be manifested in the gamma ray angular distributions, whose sharpness should decrease with increasing misalignment.

If the distribution of the angular momentum components I_x, I_y, I_z is statistical, it is straightforward to derive analytical expressions for the angular distributions.[14]

If one assumes $\sigma_x^2 = \sigma_y^2 = \sigma_z^2 = \sigma$ then an exact result can be derived.

Manifestation of shell effects on the angular-momentum transfer in deep-inelastic reactions

The presence of shell effects in deep-inelastic reactions has been the subject of numerous experimental and theoretical studies in the last several years. In a recent experiment along that line, the charge distribution as a function of Q-value was measured in the reaction $^{208}Pb + ^{208}Pb$ at 7.6 MeV/amu.[15] The observation of relatively small widths of the distributions when compared to those of similar heavy systems suggests the existence of a correlation between the net mass transfer and the closed-shell structure of the reactants. More generally, it is conceivable that this influence of the internal structure be exerted on other degrees of freedom of the reaction as well. In particular, we have explored the extent to which this argument applies to the angular-momentum-bearing rotational modes of the intermediate dinuclear complex using a very simple model.

In our calculation we describe the dinuclear complex by means of two touching spheres with spins S_1, S_2, and orbital angular momentum L. The relaxation of the rotational modes of the system as a function of interaction time is expressed by:[16]

$$S_1 + S_2 = \frac{\vartheta_1+\vartheta_2}{\vartheta_1+\vartheta_2+\mu R^2}\left(1 - e^{-t/\tau_R}\right) I \qquad (23)$$

where ϑ_1 and ϑ_2 are the moments of inertia of the nuclei, μ is the reduced mass of the system, R is the distance between centers, τ_R is the relaxation time constant, and I is the total angular momentum. For the dependence of the interaction time on I, we assume the following analytical expression:

$$t = \tau_I \ln \frac{I_{MAX}}{I} \qquad (24)$$

where I_{MAX} is the maximum angular momentum corresponding to a grazing collision and τ_I is a constant time. From eq. (23) and (24) the spin transferred to the fragments can be related to the total angular momentum:

$$\frac{I}{I_{MAX}} = \left(1 - \frac{\vartheta_1+\vartheta_2+\mu R^2}{\vartheta_1+\vartheta_2}\,\frac{S_1+S_2}{I}\right)^{\tau_R/\tau_I}$$

This relation provides a means to calculate the sum of the spins as a function of the orbital energy $E = (I - S_1 - S_2)^2/2\mu R^2$, which can be identified with the excess exit-channel kinetic energy if the radical energy is totally disipated.

The reduced orbital energy $\epsilon = E/E_{MAX}$ as a function of the reduced total spin $S = \frac{7}{2}\,\frac{(S_1+S_2)}{I_{MX}}$ is shown in Fig. 10a for a mass-symmetric system and four different values of the ratio τ_R/τ_I. Figure 10b illustrates the prediction of the model for the case in which one of the two fragments is magic and can carry only zero angular momentum (this is of course an extreme approximation). In addition to the expected effects due to closed-shell structure, we note that the slope of the curve in the quasielastic region (ϵ close to 1) is very sensitive to the parameter τ_I/τ_R. A comprehensive study of the dependence of gamma ray multiplicity M_γ upon Q-value should provide some general information on this parameter which is closely related to the relaxation time of rotational degrees of freedom.

Shell effects may be alternatively investigated by measuring the spin of the individual fragments. Our calculation indicates that for very asymmetric systems the spin of the light fragment should be very dependent on whether the heavy partner has a closed-shell structure or not. Under the same approximation made above and assuming that the rigid rotation limit is achieved we estimate ~40 percent difference in the spin of the light fragment when comparing the Kr + Au and the Kr + Pb reactions.

Finally we note that these estimated effects are related to the first moment of the spin distribution. Remarkably the calculation does not predict any noticeable effect on the variances as shown in Fig. 11.

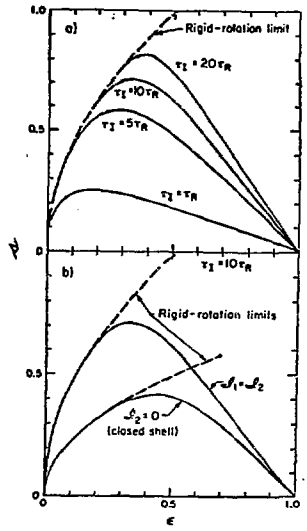

Figure 10. Reduced sum of the spins vs reduced orbital kinetic energy for a mass symmetric system, a) for different values of the ratio τ_I/τ_R and b) for two values of $\mathcal{J}_2/\mathcal{J}_1$.

Angular momentum misalignment in heavy ion reactions

An interesting measurement has been carried out for the reaction[17]) 1400 MeV $^{165}_{Ho}$ + $^{165}_{Ho}$. This system was chosen because large amounts of angular momentum can be transferred into the intrinsic spin of these nuclei, which are known to have good rotational properties. As a consequence, both of the essentially identical DI-fragments emit similar continuum γ-ray spectra which are strongly enriched in E2 transitions (80 percent).

Figure 12 (top) shows the dependence of the γ-ray multiplicity M_γ upon Q-value for three angles. Figure 10 (middle) shows the intrinsic spin of one of the two reaction fragments after neutron emission (solid line). The primary fragment spin obtained from M_γ with correction for neutron emission (dashed line) is also shown.

The ratio of in-plane to out-of-plane γ-ray yield ("anisotropy") for energies between 0.6 and 1.2 MeV is also shown in fig. 12 (bottom). This anisotropy rises with increasing spin transfer; it peaks at a value of 2.2, slightly before the spin saturates, and then drops to near unity for large Q-values.

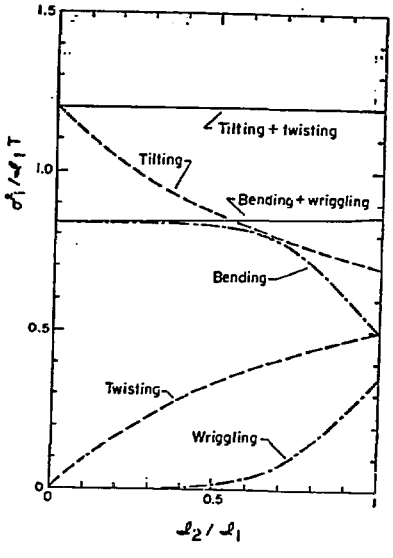

Figure 11. Fluctuations in the spin of one fragment as a function of the moment of inertia ratios of the two fragments at symmetry. The change in the ratio is to be interpreted as due to a varying degree of magicity of one of the fragments. Notice how the sum of the fluctuations is insensitive to the ratio.

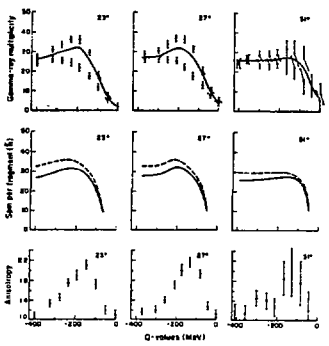

Fig. 12. Top: in-plane, out-of-plane (data points) and integrated γ-ray multiplicity as a function of Q-value for the reaction Ho + Ho at 8.5 MeV/A. Middle: spin per fragment before (dashed curve) and after (solid curve) neutron emission as a function of Q-value. Bottom: gamma-ray anisotropy as a function of Q-value.

The initial rise of the anisotropy with increasing Q-value indicates that during the early stages of energy damping there is a rapid buildup of aligned spin. The subsequent fall observed at larger Q-values suggests that the aligned component of spin has saturated or is decreasing, whereas randomly oriented components continue to increase, causing a significant decrease in the alignment of the fragments' spin.

Figure 13 shows experimental values of the anisotropy for E_γ greater than 0.6 MeV compared to several stages of the model calculation. The spin I was determined from the γ-ray multiplicity, and the anisotropy was then calculated (solid line). This calculation reproduces both the shape and the magnitude of the data. To give a feeling for the importance of various contributions, the same calculation is shown including only E1 transitions (dashed curve) and including E1 transitions and neutron emission (dotted line). This comparison clearly shows that the most important effect is the thermally induced misalignment, indicating that the decrease of alignment as deduced from the anisotropy is inherent to the deep-inelastic process itself.

A provisional conclusion is that the equilibrium statistical limit is very close to the regime controlling the spin misalignment in this reaction.

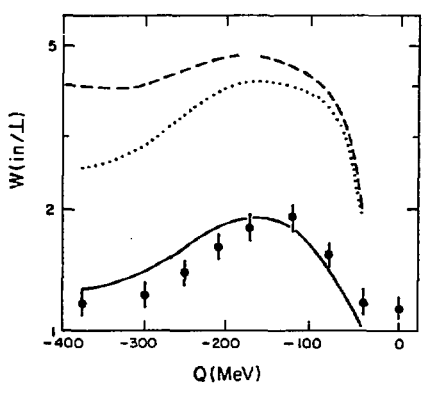

Fig. 13. Experimental and calculated (solid line) anisotropies vs Q-value. The dashed line shows the effect of E1 gamma rays alone and the dotted line shows the effect of neutron emission.

4b) ANGULAR DISTRIBUTIONS OF SEQUENTIAL FISSION FRAGMENTS

The magnitude of the transferred angular momentum and of its misalignment can be measured through the in- and out-of-plane angular distribution of sequentially emitted products. In the very asymmetric ^{20}Ne + ^{197}Au and ^{238}U systems which we have investigated[18]) the statistical excitation of a number of angular-momentum-bearing modes is strongly suppressed. In particular, the large difference in the moments of inertia of the two reaction partners increases the amount of energy necessary to excite any mode in which the small fragment is forced to rotate (wriggling, bending and twisting[3,14]).

In the statistical model, the fixed aligned components of the fragments angular momenta couple to angular momentum components associated with the internal modes of the complex causing the total fragment angular momentum to become misaligned. When the reaction partners have equal masses, the thermal widths of the angular momentum components are nearly equal in the usual cartesian coordinates (x axis taken along the line-of-centers). However, when the reaction partners have different masses, and hence different moments of inertia, the situation changes dramatically. The statistical widths of the angular momentum components in the heavy fragment generated by the normal modes are shown individually in fig. 14 as a function of mass asymmetry. An in-plane anisotropy arises when $\sigma_x^2 \neq \sigma_y^2$. This is the case at large mass asymmetries due to the fact that only the tilting mode remains active, while all the other modes are essentially frozen. Thus, very asymmetric reaction systems should provide an excellent test of the excitation of selected normal modes and of the statistical model in general.

In-plane sequential fission studies, which should be the most sensitive to differences between σ_x and σ_y, have given conflicting results. In refs. 21 and 22 an in-plane anisotropy was observed at low Q-values which diminished at high Q-values; however, no such anisotropies were found for a similar system in ref. 22. The apparent conflict notwithstanding, the mass asymmetries of all of these systems are such that the statistical model predicts $\sigma_x^2 = \sigma_y^2$ (cf. fig. 12). The ^{20}Ne + ^{197}Au and ^{238}U systems present a situation where this model predicts a strong in-plane anisotropy (2:1) which should peak perpendicular to the line-of-centers at contact.

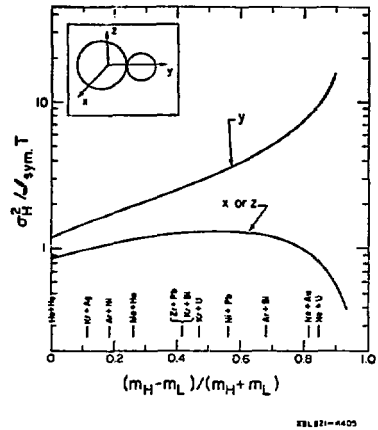

Fig. 14. The statistical widths for the normal modes of the dinuclear complex are shown as a function of mass asymmetry of the complex. The mass asymmetries associated with recent measurements of the angular distributions are also shown.

The measured angular distributions are presented in figs. 15,16 for the ^{20}Ne + ^{238}U system as a function of Q-value. The data have been integrated over the fission fragment energy and the atomic number of projectile residues ($6 \leq Z \leq 14$). The direction $\phi^H = 0$ was arbitrarily chosen to coincide with the laboratory recoil angle as is traditional. The sequential fission events observed at small Q-values have a small in-plane anisotropy. The anisotropy disappears at intermediate Q-values; however, for the most inelastic collisions a strong minimum is seen approximately perpendicular to the lab recoil direction. Statistically significant angular distributions from reactions with ^{197}Au were obtained only at large Q values. The position of the minimum and the anisotropies of these angular distributions are essentially the same as those shown for the most inelastic ^{238}U data. The results of chi-squared minimization fitting (K_o values following ref. 21) are shown by the solid curves in figs. 15 and 16 and are contained in Table 1. In fig. 17 the z components of the heavy fragment angular momentum are shown as a function of Q-value. The remarkably large values obtained for the Au target are a reflection of the fact that in such a nucleus only the highest spins lead to fission. In fig. (18) the elements of the polarization tensor P_{zz} and P_{xy} are shown as a function of Q-value. The lines correspond to calculations performed with different deformations of the fragments. In

general, the agreement is quite good if a ratio of axes 2:1 is allowed. Also the evolution of the anisotropy of the in-plane angular distributions with Q-value are in agreement with our expectations that the statistical model is valid in the long time limit.

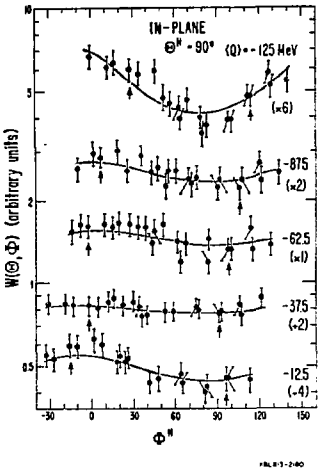

Fig. 15. The in-plane angular distributions of sequential fission fragments in the rest frame of the heavy fragment (H) are shown as a function of reaction Q-value for the ^{20}Ne + ^{238}U system. The arrows indicate the in-plane angles at which out-of-plane measurements were made. The solid curves are obtained by fitting the eq. 28 to the data in each Q-value bin.

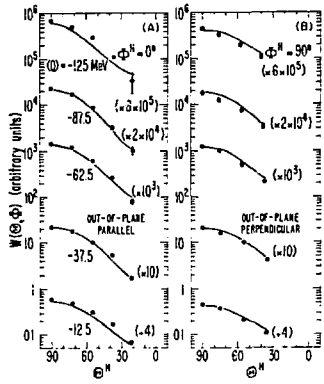

Fig. 16. The out-of-plane angular distributions that correspond to the Q-bins of Fig. 15 are shown (solid points) along with the fitted functions (solid curves).

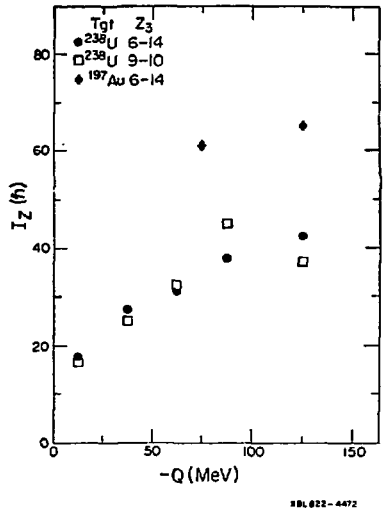

Fig. 17. The measured aligned spin (I_z) of the target-like fragment as a function of Q-value for the 252-MeV ^{20}Ne + ^{197}Au and ^{238}U reactions. Spins were extracted for a broad Z-bin (6-14) for both systems and an additional narrow one (Z = 9-10) for the ^{20}Ne + ^{238}U system. The statistical errors are of the same size or smaller than the symbols.

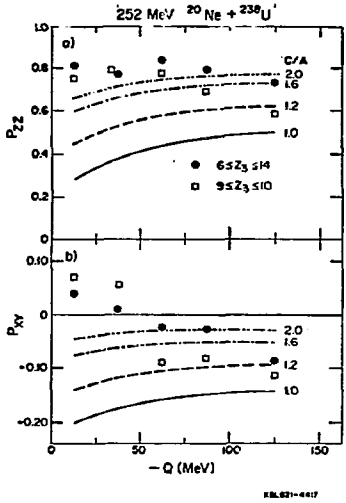

Fig. 18. The measured alignment parameters for the spin distributions obtained for the $^{20}Ne + ^{238}U$ system are shown for Z = 6 to 14 (circles) and Z = 9 and 10 (squares). The solid and dashed curves represent the statistic equilibrium model calculations (see text).

Table 1. Results of angular distribution fitting including a free rotation angle x^H, errors are given in parenthesis. The errors listed in this table represent only the statistical error.

Q-Value	K_0	I_z	σ_y	σ_x	σ_z	x^H
			(units)			(degrees)
(A) uranium results with $6 \leq Z_3 \leq 14$						
- 12.5	7.3	17.7(0.5)	3.0(0.6)	6.5(0.4)	2.8(0.4)	8.(7.)
- 37.5	10.4	27.2(0.2)	7.7(0.2)	8.9(0.2)	1.9(0.5)	16.(9.)
- 62.5	12.0	31.1(0.3)	9.5(0.5)	5.8(0.7)	3.1(0.7)	90.(9.)
- 87.5	13.1	37.9(0.3)	13.0(0.7)	8.6(0.9)	5.3(0.5)	94.(9.)
-125.	14.3	42.4(0.6)	20.1(0.7)	0.7(4.)(	9.2(1.1)	80.(3.)
(B) uranium results with $9 \leq Z_3 \leq 10$						
- 12.5	7.3	16.7(0.5)	2. (0.8)	7.1(0.4)	0.5(1.)	- 9.(6.)
- 37.5	10.4	25.0(0.3)	3.5(0.6)	10. (0.6)	7.2(0.8)	-10.(4.)
- 62.5	12.0	32.2(0.5)	17. (1.)	6. (1.)	5. (1.0)	90.(5.)
- 87.5	13.1	45. (1.)	12. (2.)	8. (2.)	15. (1.)	81.(6.)
-125.	14.3	37. (0.9)	22. (2.)	7. (2.)	0. (4.)	87.(7.)
(C) Statistical Model*						
- 12.5			16.6	5.0	5.0	45
- 37.5			21.8	6.5	5.0	60
- 62.5			24.7	7.4	7.4	70
- 87.5			26.8	8.1	8.1	75
-125.			28.8	8.8	8.8	80
(D) gold results with $6 \leq Z_3 \leq 14$						
- 75	9.8	61.(1.)	25.2(0.8)	7.(2.)	24.(1.)	64.(3.)
-125	11.7	65.(1.)	30.0(0.8)	0.(5.)	15.(1.)	79.(1.)
(E) Statistical Model*						
- 75			20.6	7.4	7.4	72
-125			23.4	8.4	8.4	80

* Two touching spheres

5. Conclusion

The relevance of statistical fluctuations to the understanding of a variety of aspects associated with deep inelastic processes has been discussed. We have argued that, wherever there is evidence for extensive relaxation, one can use the equilibrium thermal widths as good estimates of the actual widths. The equilibrium statistical limits appear to be extremely useful and should be employed to verify that the predictions of specific nonequilibrium models and their agreement with experiment are not solely associated with their correct long time limit. It may be possible to conclude tentatively that, while the whole of the deep inelastic process is clearly a nonequilibrium event, many of the involved degrees of freedom have undergone a substantial relaxation compatible with a description in terms of statistical equilibrium.

This work was supported by the Director, Office of Energy Research, Division of Nuclear Physics of the Office of High Energy and Nuclear Physics and by Nuclear Sciences of the Basic Energy Sciences Program of the U.S. Department of Energy under Contract DE-AC03-76SF00098.

References

1) R.A. Broglia, R.A. Civitarese, C.H. Dasso, and Aa. Winther, Phys. Lett. 73B (1978) 405

2) See for instance: L.G. Moretto, C.R. Albiston and G. Mantzouranis, Phys. Rev. Lett. 44 (1980) 924

3) L.G. Moretto and R.P. Schmitt, Phys. Rev. C21 (1980) 204

4) L.G. Moretto, Nucl. Phys. A247 (1975) 211

5) B. Cauvin, R. Jared, P. Russo, R.P. Schmitt, R. Babinet, and L.G. Moretto, Nucl. Phys. A301 (1977) 511

6) F. Plasil, R.L. Ferguson, H.C. Britt, R.H. Stokes, B.H. Erkkila, P.D. Goldstone, M. Blann and H.H. Gutbrod, Phys. Rev. Lett. 40 (1978) 1164

7) R.P. Schmitt, G. Bizard, G.J. Wozniak and L.G. Moretto, Phys. Rev. Lett. 41 (1978) 1152

8) B. Tamain, R. Chechik H. Fuchs, F. Hanappe, M. Morjean, C. Ngo, J. Peter, M. Dakowski, B. Lucas, C. Mazur, M. Ribrag and C. Signarbieux, Nucl. Phys. A330 (1979) 253

9) Y. Eyal, A. Gavron, I. Tserruya, Z. Fraenkel, Y. Eisen, S. Wald, R. Bass, C.R. Gould, G. Kreyling, R. Renfordt, K. Stelzer, R. Zitzmann, A. Gobbi, U. Lynen, H. Steltzer, I. Rude and R. Bock, Phys Rev. Lett. 41 (1978) 625

10) D. Hilscher, J.R. Birkelund, A.D. Hoover, W.U. Schroder, W.W. Wilcke, J.R. Huizenga, A. Mignerey, K.L. Wolf, H.F. Breuer, and V.E. Viola, Jr., Phys. Rev. C20 (1979) 576

11) L.G. Moretto, Proc. Varenna Conf., Varenna, Italy, July 9-25, 1979, in press.

12) R.P. Schmitt, G.J. Wozniak, G.V. Rattazzi, G.J. Mathews, R. Regimbart and L.G. Moretto, Phys. Rev. Lett. 46 (1981) 522

13) D.J. Morrissey and L.G. Moretto, Phys. Rev. C23 (1981) 1835

14) L.G. Moretto, S. Blau and A. Pacheco, Nucl. Phys. A364 (1981) 125

15) T. Tanabe et al., Nucl. Phys. A342 (1980) 194.

16) S. Ayik et al., Z. Phys. A286 (1978) 271.

17) G.J. Wozniak, R.J. McDonald, A. Pacheco, C.C. Hsu, D.J. Morrissey, L.G. Sobotka, L.G. Moretto, S. Shih, C. Schuck, R.M. Diamond, H. Kluge, and F.S. Stephens, Phys. Rev. Lett. 45 (1980) 1081

18) D.J. Morrissey, G.J. Wozniak, L.G. Sobotka, A.J. Pacheco, C.C. Hsu, R.J. McDonald and L.G. Moretto, LBL-12181 (March 1981)

19) L.G. Sobotka et al., Phys. Rev. Lett. in press (1981)

20) P. Dyer et al., ibid 39 (1977) 392 and Nucl. Phys. A322 (1979) 205

21) R.J. Puigh et al., Phys. Lett. 86B (1979) 24

22) D. v. Harrach et al., Phys. Rev. Lett. 42 (1979) 1728

23) C. LeBrun et al., 6th Session d'etudes Biennale de Physique Nucleaire, Aussis, France, 2-6 February 1981